Journal of Electron Devices, Vol. 22, 2015, pp. 1895-1906 **Journal of Electron Devices**
www.jeldev.org

© JED [ISSN: 1682 -3427]

[ISSN: 2412 -1150](Online)

Possible High Efficiency and RF Power Generation from n-Ge/p-Si Junction Impatt Diodes beyond 100 GHz

P. R. Tripathy[1], S. K. Choudhury[2] and S. P. Pati[3]
[1]Hi-Tech College of Engineering, Bhubaneswar, Odisha
[2]G. M. (Auto) College, Sambalpur, Odisha
[3]AICTE Emeritus Professor, NIST Berhampur, Odisha
E. Mail: pravashrt76@yahoo.co.in, skchoudhury_71@yahoo.co.in, prof_sppati@yahoo.co.in

ABSTRACT

The authors have investigated the static and dynamic performance of complementary n-Ge/p-Si heterojunction double drift ($n^{++}npp^{++}$) IMPATT diodes through advanced and realistic computer simulation techniques for operation in the F, D and G-band frequencies. The results are further compared with corresponding Si and Ge homojunction devices at the same frequency of design. The study shows high values of device efficiency, such as, 20.2 %, 19.8 % and 19.1 % for n-Ge/p-Si impatt diode as compared to Si (9.80 %, 9.36 %, 8.83 %) and Ge (12.9 %, 12.8 %, 12.0 %) at F, D and G-band, respectively. The peak device negative conductance for n-Ge/p-Si heterojunction devices are found to be 5.80×10^8 S/m^2, which are ~5-15 times than corresponding Ge (1.16×10^8 S/m^2) and Si (0.39×10^8 S/m^2) counterparts at G-band. The computed values of RF power-density for n-Ge/p-Si hetero junction IMPATTs is 15.5×10^8 W/m^2 as compared to Si and Ge-based IMPATT devices having power density as 11.8×10^8 W/m^2 and 7.08×10^8 W/m^2 at G-band operation. Hence the n-Ge/p-Si hetero-junction diode can become superior RF-power generator over a wide range of frequencies. The present study may help the device engineers to choose suitable material pair for development of high-power/high efficiency MM-wave IMPATT for communication.

Keywords: Ge/Si material systems, MM-wave high-power IMPATT device, Double Drift diode, High-efficiency, Admittance characteristics.

1. INTRODUCTION:

The advancement in solid state devices has contributed significantly towards the feasibility of high-power MM-wave sources. Among all the solid-state sources, impact avalanche transit time (IMPATT) diodes have already emerged as the most powerful solid-state source, and are now widely used in various civilian and space communication systems, as well as in high-power radars, missile seekers, etc. It is well known that the RF power depends on various factors like critical electric field for avalanche breakdown, saturation drift velocity for charge carriers, etc., which varies for different semiconductor materials and play vital role in limiting the output power of an IMPATT diode at a particular operating frequency. In the last few decades, silicon has been the basis of manufacturing a majority of semiconductor devices. But now-a-days, the conventional silicon approaches its technological dimensional limits due to its material and physical parameters. Recently, moderately wide band gap semiconductor InP and wide band gap materials such as SiC, GaN and ZnS have been proposed for fabrication of high-power MM-wave IMPATT diodes [1-4]. Even though these new class of semiconductor based IMPATTs have certain advantages, experimental success is limited due to difficulties of availability of pure crystalline material and their growth techniques for doping p and n type impurities. On the other hand, Si technology has already been reached a fair level of maturity. Moreover, compared to SiC, InP and GaN wafers, Si wafers are easily available and cost effective. This is why semiconductor devices fabricated on Si has dominated solid state electronics industry for the last three decades. The main drawbacks of conventional Si IMPATTs are its low power output and efficiency at higher MM-wave region when one goes to low dimensional width. In this paper, the authors have proposed a way to solve this problem by using a

material pair, which has distinctly different band gap energy and with tolerable lattice mismatching, for developing DDR IMPATT diodes. Recently, research and development of Si/Ge heterojunction based device has been reported [5]. The advancement in semiconductor technology has made it possible to grow thin multi layer device leading to the concept of heterojunction devices. The simulation of the dynamic properties of n-Ge/p-Si asymmetrical heterojunction IMPATTs along with Si and Ge homojunction IMPATTs are studied and compared. A generalized simulation technique developed by the authors [6] has been used for the purpose. To the best of authors' knowledge, this is the first report on heterojunction IMPATT diodes based on Si/Ge material systems beyond 100 GHz.

2. DEVICE MODELING SCHEME

The IMPATT diode is basically a p-n junction diode that operates when it is reverse-biased to avalanche breakdown condition. The schematic diagram of heterojunction IMPATT is shown in figure 1. Table 1 shows the material and physical parameters of both Ge and Si semiconductor materials. A one-dimensional model of the p-n junction has been considered in the present analysis.

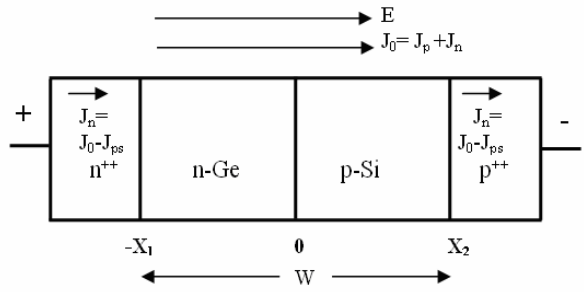

Figure 1: Schematic diagram of hetero junction n-Ge/p-Si IMPATT diode

The following assumptions have been made in the simulation of DC and small signal behavior of the DDR IMPATT diodes: (i) the electron and hole velocities have been taken to be saturated considering appropriate punch through factor and thus independent of the electric field throughout the space-charge layer, (ii) the effect of carrier space-charge has been considered, (iii) the effect of carrier diffusion has been considered, and (iv) the effect of parasitic resistance is incorporated in the analysis.

2.1 DC Analysis

The dc method, described in details elsewhere [6], considers a generalized (n^{++} n p p^{++}) structure. Here, n^{++} and p^{++} are highly doped substrates and n and p are epilayers. Summarily, in the DC method, the computation starts from the field maximum near the metallurgical junction. The distribution of dc electric field and carrier currents in the depletion layer are obtained by a double-iterative simulation method, which involves iteration over the magnitude of field maximum (E_m), and its location near the junction within the depletion layer. The method is used for a simultaneous solution of Poisson and carrier continuity equations at each point in the depletion layer. The realistic field dependence of electron and hole ionization rates, carrier mobility, and the saturated drift velocities of electron (v_{sn}) and hole (v_{sp}) in Si [7] and Ge [8] are used in the computation for the profiles of electric field and carrier currents. The RF conversion efficiency (η) [9] is calculated from the semi-quantitative formula,

$$\eta(\%) = V_D/\pi V_B \qquad (1)$$

where, V_D = voltage drop across the drift region. Also, $V_D = V_B - V_A$, where, V_A = voltage drop across the avalanche region, and, V_B = breakdown voltage. The results of the dc analysis are then used in the small signal analysis, described briefly in the next sub-section

Table 1: Physical and Material parameters of Ge and Si and semiconductor materials

Parameter	Ge	Si
Ionization coefficient of electrons at low fields, A_n ($10^8 m^{-1}$)	15.5	0.62
Ionization coefficient of electrons at low fields, B_n ($10^8 Vm^{-1}$)	1.56	1.31
Ionization coefficient of holes at low fields, A_p ($10^8 m^{-1}$)	1.0	2.0
Ionization coefficient of holes at low fields, B_p ($10^8 Vm^{-1}$)	1.28	2.17
Ionization coefficient of electrons at high fields, Ah_n ($10^8 m^{-1}$)	15.5	0.50
Ionization coefficient of electrons at high fields, Bh_n ($10^8 Vm^{-1}$)	1.56	1.22
Ionization coefficient of holes at high fields, Ah_p ($10^8 m^{-1}$)	1.0	0.56
Ionization coefficient of holes at high fields, Bh_p ($10^8 Vm^{-1}$)	1.28	1.52
Saturation drift velocity of Electron, V_{sn} ($\times 10^5$ m/s)	0.6	1.0

Saturation drift velocity of holes, V_{sp} ($\times 10^5$ m/s)	0.8	0.9
Electron Mobility, μ_n ($m^2V^{-1}S^1$)	0.039	0.15
Hole Mobility, μ_p ($m^2V^{-1}S^{-1}$)	0.019	0.06
Permittivity, ε (10^{-11} F/m)	14.1	10.1
Band Gap, E_g (eV)	0.67	1.12

2.2 Small Signal RF-Analysis

An accurate and generalized method of small signal analysis of IMPATT diodes has been presented in this section considering all the three components of carrier currents. An iterative computer simulation method is considered to study the small signal analysis [6]. The DC data obtained from DC analysis for any diode structure having a particular doping profile and operating conditions are used as input for the small signal analysis. The boundary of the edges of the depletion layer which are obtained from the DC analysis, are taken as starting and end points for the small signal analysis. The small signal analysis of the IMPATT diode provides insight into the high frequency performance of the diode [10]. The range of frequencies exhibiting negative conductance of the diode can easily be computed by Gummel-Blue method [11]. From the dc field and current profiles, the spatially dependent ionization rates that appear in the Gummel-Blue equations are evaluated, and fed as input data for the small signal analysis. The edges of the depletion layer of the diode, which are fixed by the dc analysis, are taken as the starting and end points for the small signal analysis. On splitting the diode impedance Z (x,ω) obtained from Gummel–Blue method, into its real part R (x,ω) and imaginary part X (x,ω), two differential equations are framed [12, 13]. A double-iterative simulation scheme incorporating modified Runge-Kutta method is used to solve these two equations simultaneously. The small signal integrated parameters like negative conductance (-G), susceptance (B), impedance (Z), frequency band width, and the quality factor (Q) of the diode are obtained satisfying the boundary conditions derived elsewhere [6]. The simulation method provides the high-frequency negative resistance and negative reactance profiles in the space-charge layer of the device. The diode negative resistance ($-Z_R$) and reactance ($-Z_x$) are computed through numerical integration of the -R (x) and -X (x) profiles over the active space-charge layer.

The integrated values of resistance and reactance give Z_R and Z_X using the relation,

$$Z_R = \int_0^w R(x)dx \text{ and } Z_x = \int_0^w X(x)dx \qquad (2)$$

The diode impedance Z is given by,

$$Z(\omega) = \int_{-x_1}^{x_2} Z(x,\omega) = -Z_R + jZ_X \qquad (3)$$

The diode admittance is expressed as,

$Y = 1/ Z = -G + jB = 1/ (-Z_R + j Z_X)$

or, $-G = -Z_R / ((Z_R)^2 + (Z_X)^2)$ and $B = Z_X / ((Z_R)^2 + (Z_X)^2)$ (4)

It may be noted that both –G and B are normalized to the area of the diode. Using the values of Z_R and Z_X, the diode conductance (G), susceptance (B) and the quality factor (Q) are calculated using the relation,

$$G = \frac{Z_R}{Z_R^2 + Z_x^2} \qquad B = \frac{-Z_x}{Z_R^2 + Z_x^2} \text{ and } Q = -\left|\frac{B}{G}\right|$$

The series positive resistance (R_S) of any device is one of the important limiting factors responsible for limiting power output and device efficiency [6]. This series resistance arises out of undepleted epilayer, n^+ and p^+ substrate, semiconductor metal contact, device packaging etc. Thus series positive resistance should be calculated to study its impact on device microwave performance [14]. The value of R_S can be computed from the equation [15],

$$g = -G - B^2R_S \qquad (5)$$

Under small signal condition where V_{RF} is small, the value of R_S is calculated from equation (5) by considering the value of load conductance g to be nearly equal to diode conductance [16]. The small signal analysis is repeated for different frequencies. The optimum frequency (f_p) corresponds the frequency at which the negative conductance ($-G_p$) is peaked. The values of diode negative resistance at f_p ($-Z_{Rp}$) and total negative reactance ($-Z_{Xp}$) can also be found out from the analysis. The bandwidth within which the p-n junction can generate microwave negative resistance can be determined from high frequency analysis. At a given bias current density, the peak frequency (f_p) is the frequency at which the negative conductance of the

diode is a maximum, and the quality factor is a minimum. At resonance, the power density from the device is obtained from the expression [17]: $P = (V_{RF})^2 \times G_{P.} A/2$, where V_{RF} (amplitude of the RF swing) is taken as $V_B/2$, assuming a 50% modulation of the breakdown voltage V_B. A is the area of the diode. The diode negative conductance at the optimum frequency ($-G_p$) is normalized to the area of the diode.

3. RESULTS AND DISCUSSIONS

The structural parameters of MM-wave optimized diodes are shown in table 2. Background doping concentrations and current densities are optimized for an appropriate punch-through factor [12]. Doping concentration versus Breakdown voltage for n-Ge/p-Si based DDR IMPATT diode is shown in figure 2. From figure 2 it is shown that breakdown voltage is decrease and the doping is increase. The design Frequency versus Breakdown voltage and efficiency of Si, Ge and n-Ge/p-Si DDR Impatt diode is shown in figure 3. It is observed that the breakdown voltage is higher in Si homojunction devices.

Table 2: Design Parameters of Si, Ge and n-Ge/p-Si based MM-wave IMPATTs

Design Frequency (GHz)	Structural parameters	Si (Homo-junction)	Ge (Homo-junction)	(n-)Ge/(p-)Si (Hetero-junction)
104.0	Background doping concentration (n-side) (10^{23} m^{-3})	1.8	0.9	1.9
	Background doping concentration (p-side)(10^{23} m^{-3})	1.8	1.0	1.6
	Depletion region width (n-side) (micron)	0.3	0.26	0.15
	Depletion region width (p-side) (micron)	0.3	0.24	0.16
	Bias current density (10^8 A/m^2)	6.0	50	1.00
	Substrate doping concentration (10^{26} m^{-3})	1.0	1.0	1.0
140.0	Background doping concentration (n-side)(10^{23} m^{-3})	3.0	1.0	2.6
	Background doping concentration (p-side)(10^{23} m^{-3})	3.0	1.0	2.2
	Depletion region width (n-side) (micron)	0.18	0.25	0.11
	Depletion region width (p-side) (micron)	0.18	0.25	0.12
	Bias current density (10^8 A/m^2)	7.0	2.2	2.0
	Substrate doping concentration (10^{26} m^{-3})	1.0	1.1	1.0
180.0	Background doping concentration (n-side)(10^{23} m^{-3})	4.8	1.6	3.9
	Background doping concentration (p-side)(10^{23} m^{-3})	4.8	1.6	3.3
	Depletion region width (n-side) (micron)	0.14	0.17	0.083
	Depletion region width (p-side) (micron)	0.14	0.17	0.085
	Bias current density (10^8 A/m^2)	9.5	3.0	2.5
	Substrate doping concentration (10^{26} m^{-3})	1.0	1.1	1.0

The electric field profiles of the diodes at F-band, D-band and G-band are shown in Figures 4(a-c). It is observed from the figures that in each case, electric field maximum in homojunction Si IMPATTs are higher than other diodes. The same observation is reflected in table 2, where the DC and high-frequency properties of the different IMPATT diodes at F-band, D-band and G-band are depicted. These values are higher than its Ge and n-Ge/p-Si counterparts. However, it is very interesting to note that in case of n-Ge/p-Si heterojunction diodes, voltage across avalanche region (V_A) has been decreased significantly.

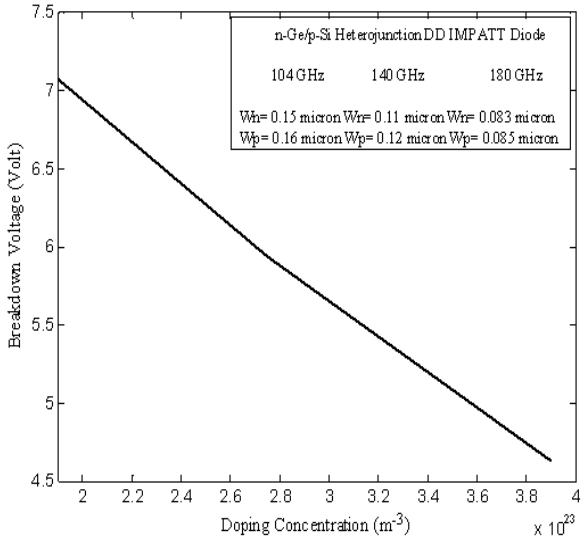

Figure 2: Plot of Doping concentration versus Breakdown voltage for n-Ge/p-Si based DDR IMPATT diode at F, D and G band frequencies

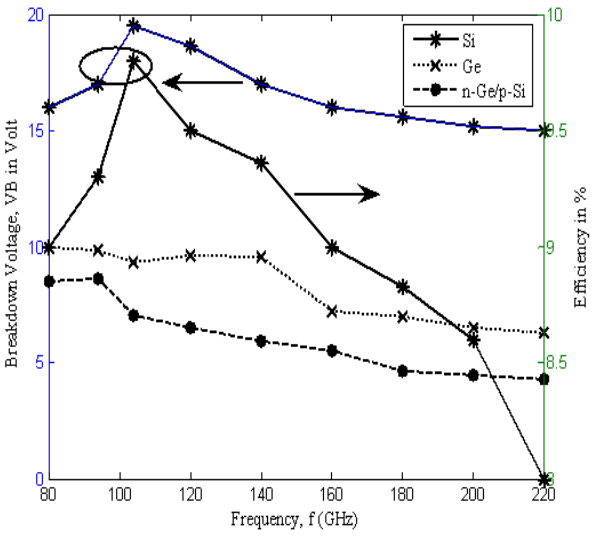

Figure 3: Plots of Frequency versus Breakdown voltage and efficiency of Si, Ge and n-Ge/p-Si DDR Impatt diode

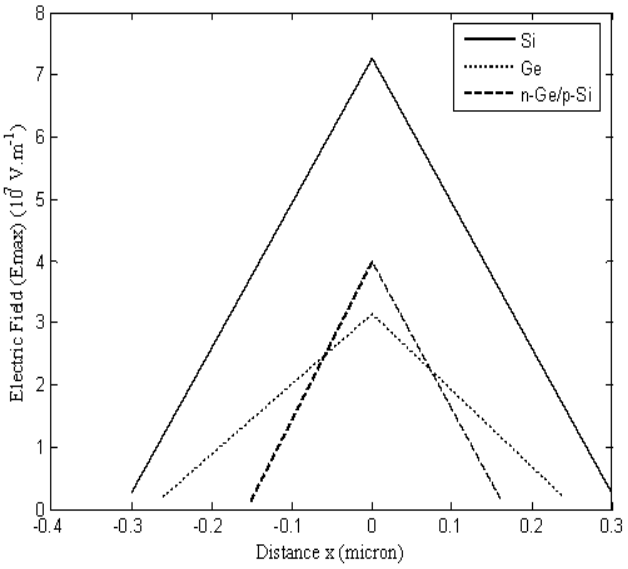

Figure 4 (a): Electric field profiles of heterojunction and homojunction IMPATT diodes at F-band

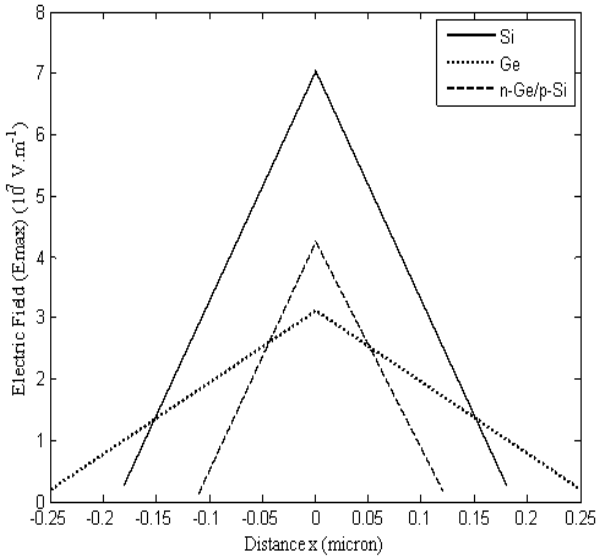

Figure 4 (b): Electric field profiles of heterojunction and homojunction IMPATT diodes at D-band

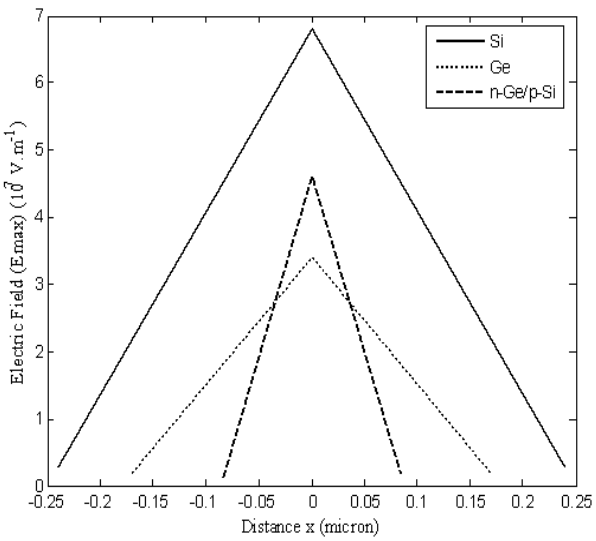

Figure 4 (c): Electric field profiles of heterojunction and homojunction IMPATT diodes at G-band

The x_A/W and V_A in case of n-Ge/p-Si hetero junction becomes the minimum as high value of hole ionization rate in Ge augments charge multiplication process and therefore localizes the avalanche zone in hole initiated n-Ge layer of this hetero junction. This reduction of V_A, increases drift voltage drop in case of heterojunction IMPATTs which in turn increases efficiency. From the simulation studies it is clear that in case of heterojunction diodes normalized drift voltage drop is quite high than its homojunction counterparts. It is found that in n-Ge/p-Si IMPATTs normalized drift voltage drop is 63.5% at F-band, 62.2% at D-band and 60.0% at G-band, which are significantly higher than those in Si and Ge homojunction diodes, as shown in table 2. The study depicts that for F-, D- and G-band operation, device efficiencies are 20.2%, 19.8% and 19.1%, respectively for n-Ge/p-Si IMPATTs. So, in terms of RF conversion efficiency, heterojunction IMPATTs are performing much better than their homojunction counterparts at all the three important MM-wave frequency bands shown in figure 3. It is observed from the figure 5 at all the three frequency bands; negative conductance is much higher in heterojunction diodes than in homojunction diodes. Negative conductance of all the diodes increases initially up to peak operating frequency, then it decreases as expected. Figure 6 compares the admittance characteristics of n-Ge/p-Si diode at F-band, D-band and G-band. Diode susceptance is increasing continuously with frequency. It is interesting to find from table 2 that the quality factor of the diodes improves (becomes low) significantly when we are using heterojunction diodes. This indicates that in the MM-wave region, signal generation stability from heterojunction IMPATTs will be far better than their homojunction counterparts. The variation of RF power density with frequency for all the MM-wave diodes are shown in Figure 7. It is interesting to observe that n-Ge/p-Si heterojunction IMPATT may produce 15.5×10^8 W/m^2 of RF power densities at G-band, which are much higher than Si (11.8×10^8 W/m^2) and Ge (7.08×10^8 W/m^2) due to high negative conductance even if the breakdown voltage is low. But at F-band and D-band the power density of Si is more due to its high breakdown voltage. Thus in terms of power output and efficiency, heterojunction IMPATTs, particularly n-Ge/p-Si heterojunction diode is performing much better than others. Variation of impedance versus frequency of DDR Heterojunction devices are shown in figures 8(a-c) for F-band, D-band and G-band operation. Figure 9 shows the Positive series resistance versus frequency of DDR Heterojunction (n-Ge/p-Si) Impatt diode. From this figure and table 2, it shows that the positive resistance Rs value is decreasing when the frequency increases. The results mentioned here may provide due impetus for fabrication of hetero junction IMPATTs for operation in the MM-wave range.

Table 3: Simulation results of Ge, Si and n-Ge/p-Si based IMPATTs

Design frequency (GHz)	DDR IMPATTs based on	DC Results					High-frequency Results					
		V_B (V)	V_A (V)	V_D/V_B (%)	E_{max} (10^7 V/m)	η (%)	f_P (GHz)	$-G_P$ (10^8 Sm^{-2})	$-Q_P$	Power Density, P ($\times 10^8$ W/m^2)	$-Z_{RP}$ (10^{-8} Ω m^2)	$+R_S$ (10^{-9} Ωm^2)
104.0	Si (Homo-junction)	19.5	13.6	30.2	7.26	9.80	104.0	0.42	3.3	19.9	0.68	1.5
	Ge (Homo-junction)	9.31	5.55	40.38	3.15	12.9	105.0	0.27	4.2	2.92	0.04	0.631
	(n-)Ge/(p-)Si (Hetero-junction)	7.07	2.58	63.5	3.99	20.2	105.0	1.86	0.8	11.6	0.31	1.12
140.0	Si (Homo-junction)	17.0	11.9	29.4	7.03	9.36	138.0	0.52	6.1	18.7	0.41	0.78
	Ge (Homo-junction)	9.59	5.75	40.0	3.13	12.8	140.0	0.64	7.3	7.35	0.18	0.312
	(n-)Ge/(p-)Si (Hetero-junction)	5.93	2.24	62.2	4.24	19.8	143.0	3.36	0.7	14.7	0.17	0.606
180.0	Si (Homo-junction)	15.6	11.4	26.9	6.80	8.83	178.0	0.39	8.5	11.8	0.28	0.38
	Ge (Homo-junction)	6.99	4.35	37.0	3.41	12.0	183.0	1.16	9.8	7.08	0.09	0.162
	(n-)Ge/(p-)Si (Hetero-junction)	4.63	1.85	60.0	4.62	19.1	180.0	5.80	0.6	15.5	0.10	0.433

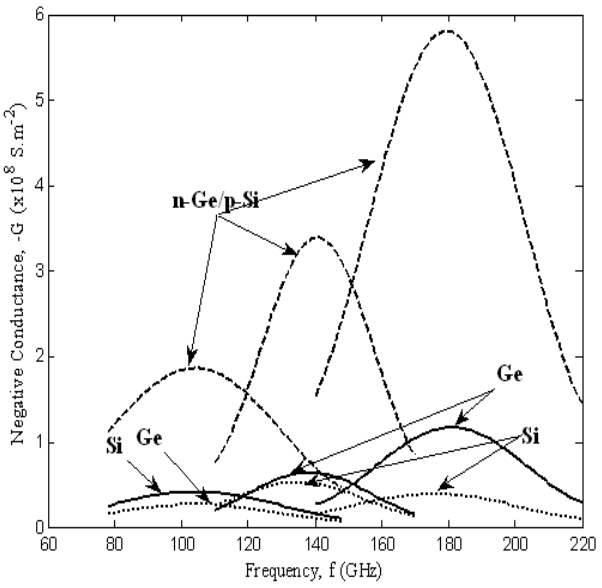

Figure 5: Plot of Negative Conductance versus Frequency for Ge, Si and n-Ge/p-Si based DDR IMPATT diode at F, D and G band frequencies

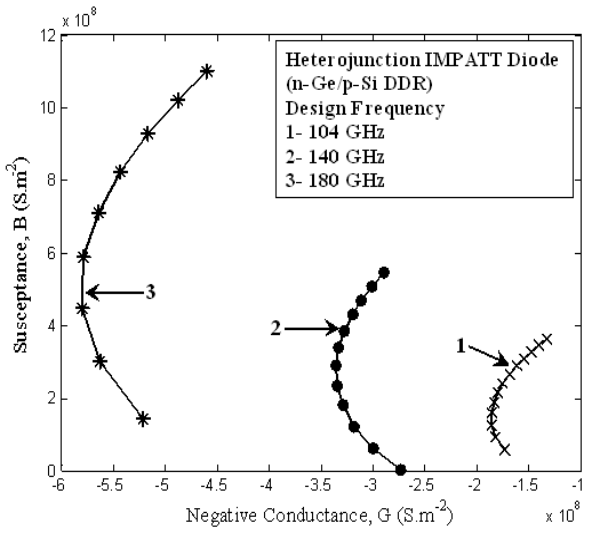

Figure 6: Plot of Negative Conductance versus Susceptance for n-Ge/p-Si based DDR IMPATT diode at F, D and G band frequencies

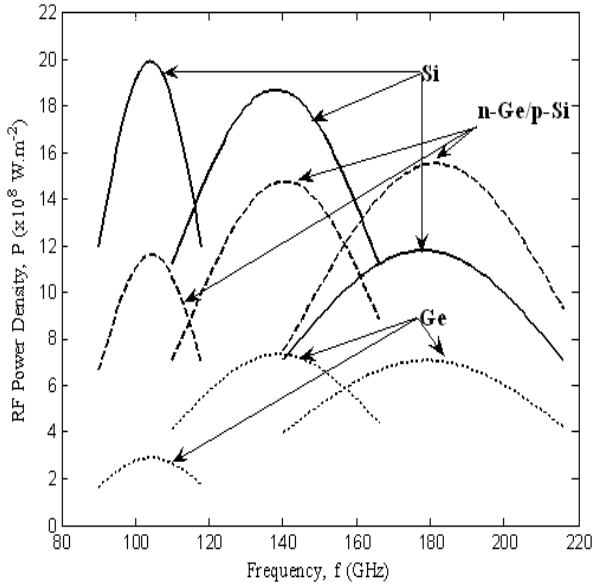

Figure 7: Variation of RF power density with frequency for Si, Ge and n-Ge/p-Si based DDR at F, D and G band frequencies

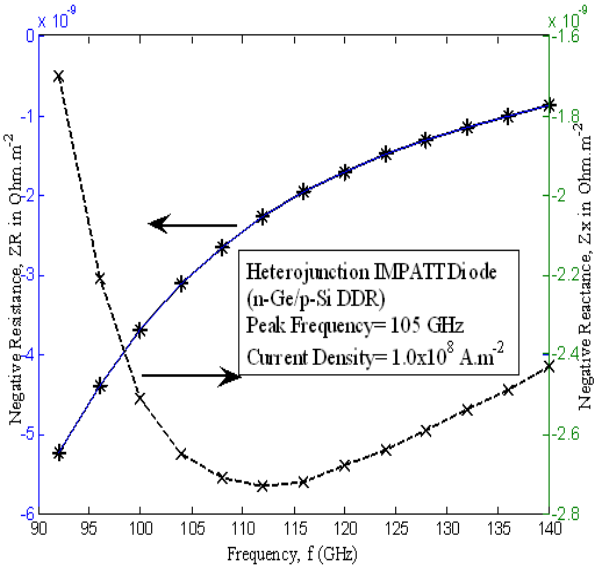

Figure 8 (a): Plots of the variation of impedance versus frequency of DDR Heterojunction (n-Ge/p-Si) Impatt diode at F- band

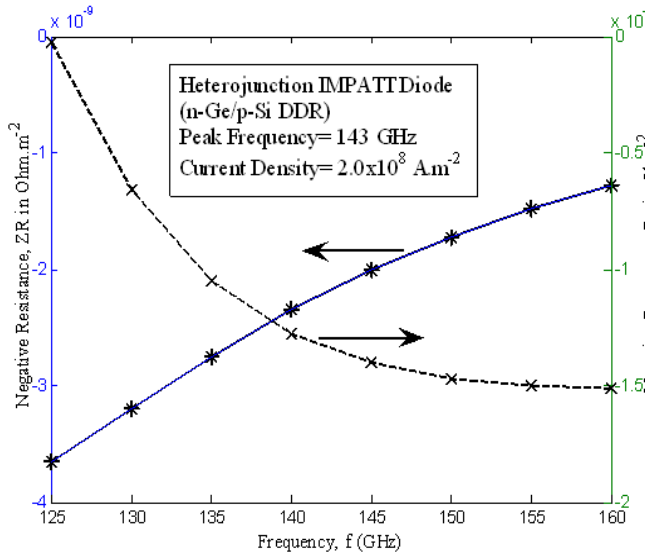

Figure 8 (b): Plots of the variation of impedance versus frequency of DDR Heterojunction (n-Ge/p-Si) Impatt diode at D- band

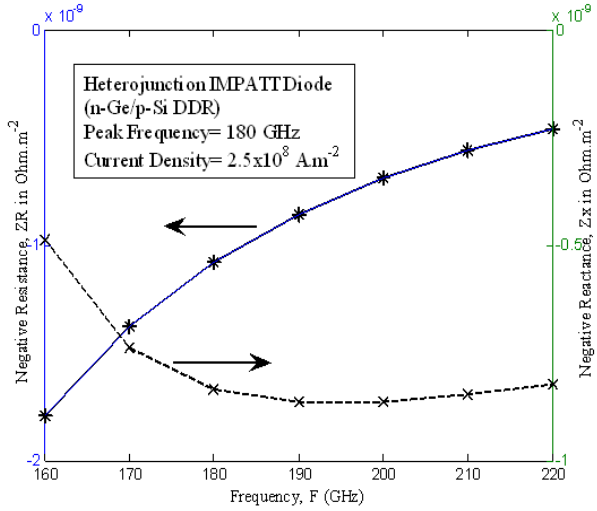

Figure 8 (c): Plots of the variation of impedance versus frequency of DDR Heterojunction (n-Ge/p-Si) Impatt diode at G- band

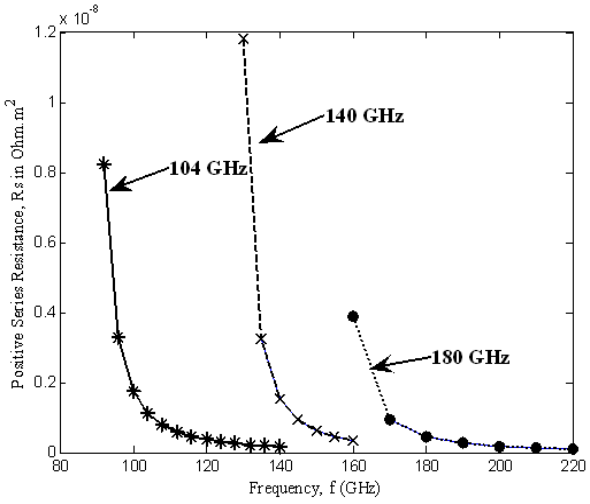

Figure 9: Plots of Positive series resistance versus frequency of DDR Heterojunction (n-Ge/p-Si) Impatt diode

4. PROPOSED FABRICATION TECHNIQUES

Si/Ge hetero-junction diode has been fabricated by depositing p-Ge thin films on n-Si substrates using molecular beam epitaxy and electron beam evaporation techniques [18]. The fabrication simplicity and absence of high-temperature diffusion processes may be taken as favorable parameters for n-Ge/p-Si hetero-junction devices for using them as detectors in the visible and IR ranges: 500 to 1800 nm. Reports indicate that the crystal mismatch (about 4.2%) between Ge and Si can be reduced by varying the Ge proportion layer width in Ge_xSi_{1-x} and $Ge_{1-x}C_x$ combinations as well as by post-deposition thermal annealing [19]. Ge films (100-200 nm thick) can be deposited on n-type Silicon substrates (ρ: 1.5 – 20 ohm.cm) by both E-beam evaporation (CHA: base pressure of 3×10^{-6} Torr), and Molecular Beam Epitaxy (MBE: base pressure 8×10^{-6} Torr). The films were found to be p-doped (ρ: 0.06 – 1 ohm.cm), as grown. The growth temperature for MBE and E-beam evaporation is 375 ± 25^0C and 300 ± 10^0C respectively. The growth of Ge on Si, using MBE, can be monitored by Reflection High Energy Electron Diffraction (RHEED). The crystal quality and strain of grown Ge/Si structures is probed by *ex situ* x-ray diffraction (both θ - 2θ and rocking curves) using $CuK\alpha_1$ (1. 5406 A^0) radiation in a double-axis Bede3 diffractometer. The electrical and optical properties of both large (5mm × 5mm) and 200 μm × 200 μm mesa p-n junctions have been also studied. Ohmic contacts are made on the Si through Ti/Al and on Ge using silver and Au/Pd [20]. The etch pit density is

significantly lower in the MBE samples ($5\times10^8/cm^2$) compared to E-beam samples ($2\times10^{10}/cm^2$). The appreciable performance of the p-n junction diode is expected to provide a drive for fabrication of heterojunction based IMPATT diode.

5. CONCLUSION

The study throws light on the static and dynamic characteristics of Si, Ge and Ge/Si IMPATT diodes. The complementary heterojunction diode structures may be taken as better RF generators compared to homo junction Si and Ge IMPATTs. It is observed that MM-wave performance of n-Ge/p-Si hetero-junction IMPATT may become the best and thus would become an extremely useful for MM-wave power generation at F-band, D-band and G-band frequencies.

REFERENCES

[1] M. Mukherjee, N. Mazumder and A. Dasgupta, "Simulation experiment on optical modulation of 4H-SiC millimeter-wave high power IMPATT Oscillator", J. of the European Microwave Association (EuMA Publishing - UK), 4, 276-282, (2008).

[2] M. Mukherjee, N. Mazumder, "Effect of charge-bump on high-frequency characteristics of α-SiC based double drift ATT diodes at MM-wave window frequencies", IETE Jr. of Research (IETE Publishing, India, 55,118 -127 (2009).

[3] M. Mukherjee, P. Tripathy and S. P. Pati, "Effects of mobile space-charge on dynamic characteristics and parasitic resistance of InP Terahertz IMPATT oscillator operating at elevated junction temperature", Archives of Applied Science Research 2, 42-52 (2010).

[4] S. P. Pati, P. R. Tripathy and S. K. Dash, "Avalanche Breakdown Characteristics of Wide Band Gap vis-à-vis Low Band Gap Junctions and High RF Power/Low Noise Generation in ZnS DD IMPATTs", International Journal of Pure and Applied Physics 6, 229-241(2010).

[5] H. Kanbe, M. Miyaji and T. Ito, "Ge/Si Heterojunction Photodiodes Fabricated by Low Temperature Wafer Bonding", Applied Physics Express 1, 072301-072303, (2008).

[6] Moumita Mukherjee, Pravash R. Tripathy and S. P. Pati, "Asymmetrical homojunction and heterojunction Transit Time Devices based on Si/Ge and Ge/Si material systems-A comparative analysis at MM-Wave frequencies", *Journal of Semiconductors*, Vol. 32, No. 11, pp. 113001-1 to 7, (2011).

[7] Electronic Archive: New Semiconductor Materials, Characteristics and Properties (Online) www.ioffe.ru/SVA/NSM/Semicond/Si

[8] T. Mikawa, S. Kagawa, T. Kaneda, Y. Toyoma, and O. Mikami, "Crystal orientation dependence of ionization rates in germanium," Appl. Phys. Lett, 37, 387–9 (1980).

[9] D. L. Scharfetter and H. K. Gummel, "Large signal analysis of a silicon Read diode oscillator", IEEE Trans. Electron Devices 16, 64-77 (1969).

[10] G. N. Dash, and S. P. Pati, "Small signal computer simulation of IMPATT diodes including carrier diffusion", *Semiconductor Sc. & Tech.*, Vol. 6, pp. 348-355 (1991).

[11] H. K. Gummel and J. L. Blue, "A small signal theory of avalanche noise in IMPATT Diodes", IEEE Trans. Electron Devices, ED –14 569-580, (1967).

[12] S. K. Roy, J.P. Banerjee and S. P. Pati ," A Computer analysis of the distribution of high frequency negative resistance in the depletion layer of IMPATT Diodes", Proc.4th Conf. on Num.Anal. of Semiconductor Devices (NASECODE IV) (Dublin) (Dublin: Boole), pp. 494-500, (1985).

[13] S. P. Pati, P. R. Tripathy, S. K. Dash, S. K. Choudhury, P. Purohit, A. K. Panda and J. Majhi, "Mathematical Analysis and Realistic Simulation Modeling for Thin Impatt Devices", Proc. MATEIT-2010, Jan., 10, New Delhi.

[14] A. Acharyya et al, "Effect of Package Parasitics on the millimeter-wave performance of DDR Silicon IMPATT device operating at W-band", Journal of Electron Devices, Vol. 13, pp. 960-964 (2012).

[15] M. G. Adlerstein, L. H. Holway and S. L. G Chu, "Measurement of series resistance in IMPATT

diode", *IEEE Trans on Electron Devices*, Vol ED-30, pp.179-182 (1983)

[16] P. De, "Computer simulation method for the determination of series resistance of Si n^+np^+ SDR of X-band of operation", *Int J. Electron*, Vol-81, No.5, p.545-550 (1996)

[17] H. Eisele and G.I.Haddad, "Microwave Semiconductor Device Physics", Ed. S. M. Sze, Wiley, New York, p. 343 (1997).

[18] Prabhakar Bandaru, Subal Sahni, Eli Yablonovitch, Hyung-Jun Kim and Ya-Hong Xie, " The fabrication of p-Ge/n-Si photodetectors, compatible with back-end Si CMOS processing,by low temperature (< 400^0C) molecular beam epitaxy and electron-beam evaporation, Mat. Res. Soc. Symp. Proc. 796, V2.8.1-V2.8.6 (2004).

[19] P. R. Bandaru, S. Sahni, E. Yablonovitch, J. Liu, H.-Jun Kim, Y.-H. Xie, "Fabrication and characterization of low temperature (<450^0C) grown p-Ge/n-Si photodetectors for silicon based photonics", Material Science Engineering *B* 113, 79-84(2004).

[20] Raid A. Ismail1, Jospen Koshapa, Omar A. Abdulrazaq, "Ge/Si heterojunction photodetector for 1.064 μm laser pulses" Internation Journal of Semiconductor Physics, Quantum Electronics & Optoelectronics, 9, 49-52 (2006).